CrystEngComm

Cite this: *CrystEngComm*, 2011, **13**, 2758

www.rsc.org/crystengcomm

PAPER

Ultrasound assisted self-assembly of a BaF_2 hollow nest-like nanostructure

Jun Geng,[ab] Fang Jiang,[b] Qian Lu[b] and Jun-Jie Zhu*[b]

Received 3rd November 2010, Accepted 10th February 2011
DOI: 10.1039/c0ce00809e

A BaF_2 hollow nest-like nanostructure has been successfully synthesized, for the first time, *via* a facile sonochemical route from aqueous solution using EDTA as complexing reagent and CTAB as surfactant. Reaction conditions, such as concentrations of complexing reagent and surfactant, were found to have a close relation to the morphologies of final products. The ultrasound-induced self-assembly growth procedure has been proposed for the possible formation mechanism. The BaF_2 hollow structures showed enhanced photoluminescence compared to the solid structure.

1. Introduction

Self-assembled nanostructures with specific morphology and novel properties have attracted much attention in recent years. As a result of the rapid development of synthetic strategies, highly organized superstructures of metals,[1] semiconductors[2] and hybrid materials[3] have been fabricated *via* various methods. Among these approaches, the ultrasonic technique has been proved to be a unique tool for the growth of materials with novel structures.[4] Ultrasound provides an unusual sonochemical mechanism for generating high-energy chemistry with extremely high local temperatures, high pressures, and extraordinary cooling rates.

As one of the dielectric fluorides (along with CaF_2 and SrF_2), barium fluoride (BaF_2) has a wide range of potential applications in microelectronic and optoelectronic devices, such as wide-gap insulating overlayers, gate dielectrics, insulators and buffer layers in semiconductor-on-insulator structures, and more advanced three dimensional structure devices.[5] BaF_2 doped with rare-earth ions has been reported to display unique luminescent properties and can be used as X-ray storage phosphors, scintillators, as well as up- and down-conversion, and ionic conductivity materials.[6]

Compared with other photoluminescent nanomaterials, the morphology controlled synthesis of BaF_2 is not abundant. So far, some chemical synthetic methods have been developed to prepare BaF_2 nanostructures. For example, BaF_2 whiskers were prepared *via* a microemulsion-mediated hydrothermal method,[7] BaF_2 nanocubes with arching flake-like dendrites were grown from reverse micelles,[8] BaF_2 nanocubes of different sizes were prepared through a simple hydrothermal precipitation procedure,[9] uniform cubic-phase BaF_2 nanoparticles and orthorhombic-phase BaF_2 nanorods were prepared and self-assembled by the liquid–solid–solution (LSS) approach.[10] To the best of our knowledge, there has been no report on the preparation of BaF_2 hollow nanostructures to date. However, hollow structures may have many unique properties and have attracted great attention due to their widespread potential applications in catalysis, drug delivery, lightweight filler, acoustic insulation, photonic crystals,[11] and so on. The hollow crystals are expected to exhibit high light-collection efficiency and enhanced luminescence performance due to their hollow structures and large internal surface area at their interior.[12] Therefore, the development of methods for the synthesis of fluoride hollow nanostructures is a major challenge. It is desirable to fabricate nanophase BaF_2 with modulated hollow morphologies to enhance their special performance.

Herein, we report the synthesis of a BaF_2 hollow nest-like nanostructure *via* a facile sonochemical route with EDTA as complexing reagent and CTAB as surfactant. The reaction conditions were investigated in detail. An ultrasound-assisted self-assembly formation procedure was proposed for the possible crystal growth mechanism. It is exciting that the as-prepared BaF_2 hollow structure shows much enhanced room-temperature photoluminescence compared to the solid structure.

2. Experimental section

All of the reagents used were of analytical purity and used without further purification. $Ba(NO_3)_2$, NH_4F, ethylenediamine tetraacetic acid disodium salt (Na_2EDTA) and cetyltrimethylammonium bromide (CTAB) were purchased from Shanghai Second Chemical Reagent Factory (China). Absolute ethanol was purchased from Nanjing Chemical Reagent Factory (China).

In a typical procedure, $Ba(NO_3)_2$ (5 mmol) was dissolved in 50 mL aqueous solution, then EDTA (5 mmol) was introduced with stirring to form a clear solution. NH_4F (5 mmol) was dissolved in another 50 mL of an aqueous solution containing 0.5 g CTAB. The two solutions were mixed together in a 150 mL round-bottom flask to give a transparent reaction solution. Then the

[a]*Department of Chemistry, Jiangsu Institute of Education, Nanjing, 210013, P. R. China*
[b]*Key Laboratory of Analytical Chemistry for Life Science, School of Chemistry and Chemical Engineering, Nanjing University, Nanjing, 210093, P. R. China*

solution was exposed to high-intensity ultrasound irradiation under ambient air for 1.5 h. Ultrasound irradiation was accomplished with a high-intensity ultrasonic probe (Xinzhi. Co., China, JY92-2D, 0.6 cm diameter; Ti-horn, 20 kHz, 60 W cm^{-2}) immersed directly in the reaction solution. A white precipitate was centrifuged, washed with distilled water and absolute ethanol in sequence, and finally dried in air. The final products were collected for characterization. The products were characterized by X-ray powder diffraction (XRD), transmission electron microscopy (TEM), selected area electron diffraction (SAED), scanning electron micrographs (SEM), high-resolution transmission electron micrographs (HRTEM), and photoluminescence spectra (PL).

The XRD analysis was performed using a Philips X'-pert X-ray diffractometer at a scanning rate of 4° min^{-1} in the 2θ range from 10° to 80°, with graphite monochromatized Cu K_α radiation ($\lambda = 0.15418$ nm). SEM images were taken on a LEO-1530VP field-emission scanning electron microscope. TEM and SAED patterns were recorded on a JEOLJEM 200CX transmission electron microscope, using an accelerating voltage of 200 kV. HRTEM were obtained by employing a JEOL-2010 high-resolution transmission electron microscope with a 200 kV accelerating voltage. PL spectra were measured on a SLM48000DSCF/AB2 fluorescence spectrometer made by American SLM Incorporation at room temperature.

3. Results and discussion

3.1 Characterization of final products

Fig. 1 shows the XRD pattern of the as-prepared BaF_2 product. The obtained BaF_2 sample is of cubic structure (face-centered lattice, space group *Fm*3*m*). All the diffraction peaks can be indexed to a pure cubic structure with cell parameters $a = 6.20$ Å, which are in good agreement with the literature values (JCPDS Card No. 04-0452). The apparent broadening of the diffraction peaks indicates that the samples are composed of nanoparticles.

The morphologies of BaF_2 samples were observed with SEM and TEM techniques. Fig. 2a and b show the typical SEM images of the as-prepared BaF_2 nanocrystals. It is clearly demonstrated that the crystals have a special hollow nest-like structure with outer diameter of 900 nm and inner diameter of about 250 nm. The shells of the hollow structures seemed to be composed of flake-like building blocks. The morphology and microstructure of the as-synthesized BaF_2 hollow crystals were further studied by TEM and HRTEM. Fig. 2c shows that the as-prepared BaF_2 sample appeared as hollow nanospheres with diameter of *ca.* 900 nm. As shown in Fig. 2c and d, a strong contrast difference between the edges (dark) and centers (bright) indicates hollow interiors with a wall thickness of about 300 nm. The SAED pattern of the structures shows that the BaF_2 hollow structure is of poly-crystal nature (inset of Fig. 2d). HRTEM images provide further insight into their structures. Small flakes could be detected in the shell structure (Fig. 3e). The HRTEM image obtained on the surface of a sphere (Fig. 3f) indicates clear interplanar spacing of 0.31 and 0.36 nm, corresponding to the (200) and (111) crystal faces, respectively.

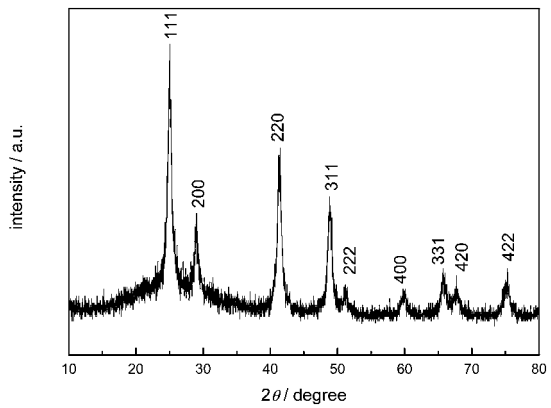

Fig. 1 X-ray diffraction pattern of the as-prepared BaF_2 nanostructure

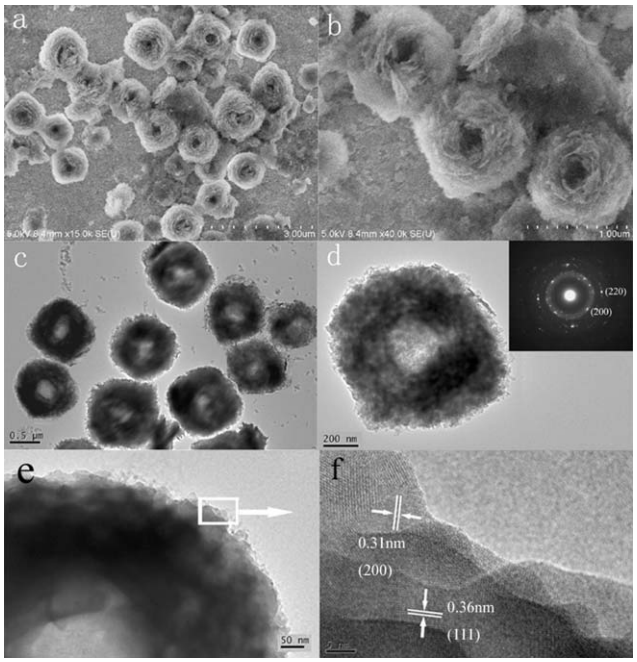

Fig. 2 (a, b) SEM images, (c, d) TEM images of the as-prepared BaF_2 hollow nanostructure, and (e, f) HRTEM images recorded on the shell of one spherical structure (the inset of Fig. 2d is the SAED pattern recorded on a single hollow sphere).

3.2 Sonochemical formation mechanism

The complexing reagent, surfactant and ultrasonic irradiation are key factors in the synthesis. EDTA is a strong coordinating reagent,[13] which can modify the growth rates of many crystals through controlling the metal ions release speed and binding crystal facets. As a result, the growth in the specific directions was retarded and thus led to anisotropic growth.[14] The formation mechanism of BaF_2 nanocrystals is probably related to the coordination of Ba^{2+} and EDTA to form a Ba-EDTA complex, and the dissociation of the complex under sonication to form BaF_2 nanocrystals. The probable reaction process in aqueous solution can be summarized as follows:

$$\text{Ba-EDTA} \rightarrow Ba^{2+} + EDTA^{2-} \quad (1)$$

$$Ba^{2+} + 2F^- \rightarrow BaF_2 \quad (2)$$

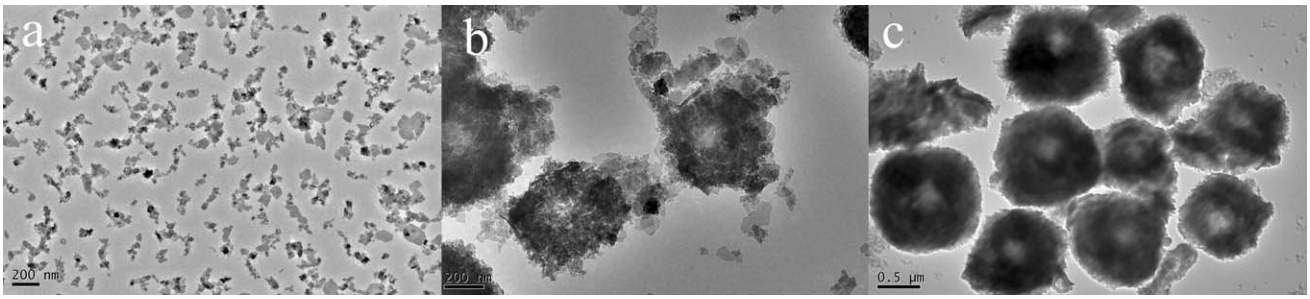

Fig. 3 TEM images of BaF_2 samples obtained after sonication for (a) 20, (b) 50, and (c) 80 min.

An ultrasound wave that is intense enough to produce cavitation can drive chemical reactions such as oxidation, reduction, dissolution and decomposition.[15] So under ultrasonic treatment the complex dissociated and *in situ* generated Ba^{2+}. The concentration of coordinating reagent would affect the release speed and the monomer concentration of free Ba^{2+} in the solution. Then F^- ions in the solution combined with the released Ba^{2+} ions to yield BaF_2 nuclei. These freshly formed nuclei are unstable and have the tendency to grow into larger grains due to their high chemical potential.[16]

In the further crystal growth process, the surfactant CTAB plays an important role in directing the growth and self-assembly of the BaF_2 nuclei to form unique hollow structure. Careful observation revealed that the hollow nest-like nanostructures were composed of small nanoflakes, as shown in Fig. 2b. In this case, due to the selective interaction between surfactant CTAB and the different crystallographic planes of BaF_2 nanocrystals, BaF_2 nuclei could grow along the preferred orientation of [100] and [110] directions and result in the formation of BaF_2 nanoflakes.[9,10] The selective adsorption of surfactants and the crystal-plane-dependent surface energy were also used to synthesize the platelike gold particles.[17]

The transient high-temperature and high-pressure field produced during ultrasound irradiation provides a favorable environment for the anisotropic growth of nanocrystals. Cavitation and shock waves created by ultrasound can accelerate solid particles to high velocities leading to interparticle collisions and inducing effective fusion at the point of collision.[18] We consider that ultrasound caused the fusion of adjacent BaF_2 nanoflakes and the attachment of primary particles on the intermediate spherical aggregates, which finally led to the hollow nest-like structure. High-intensity ultrasound irradiation was found to be necessary for the shape-controlled synthesis because comparative experiments under vigorous electric stirring instead of ultrasound treatment could not obtain the same hollow structures. The special sonochemical effect together with the influence of EDTA and CTAB resulted in the final hollow nest-like nanostructure.

To further investigate the details of the formation procedure, the growth processes of the final products were carefully followed by time-dependent experiments. TEM images obtained after different reaction times show an obvious growth process from small primary nanoflakes to spherical self-assemblies, then to the final hollow products (Fig. 3). Small primary flakes with average diameter of about tens of nanometres were observed in the early reaction time of 20 min (Fig. 3a). The self-assemblies of these nanoflakes forming hollow spherical structures could be clearly detected with further sonication for 30 min (Fig. 3b). Another sonication for 30 min gave the final hollow nest-like structure (Fig. 3c). The formation process of the specific nanostructures is schematically illustrated in Fig. 4. According to the above results, it may be concluded that the collaborative action of complexing agent, surfactant and sonication play a key role in the formation of the hollow BaF_2 nanonests.

3.3 Effect of EDTA concentration

As discussed above, EDTA plays a critical role in the formation of BaF_2 hollow nanostructures. In the system without EDTA (reaction system only containing 5 mmol $Ba(NO_3)_2$, 5 mmol NH_4F and 0.5 g CTAB), the BaF_2 products appeared as cubic in shape, as shown in Fig. 5a and b. The size of the BaF_2 cubes is about 500 nm and careful observation shows that these cubes are composed of nanoflakes. This experimental results revealed that EDTA was the key factor for the hollow structure formation and CTAB acted as a structure-directing agent to form nanoflakes through adsorption or a micelle template. The relative specific surface energies associated with the crystal facets determine the cubic shape of the BaF_2 crystals.

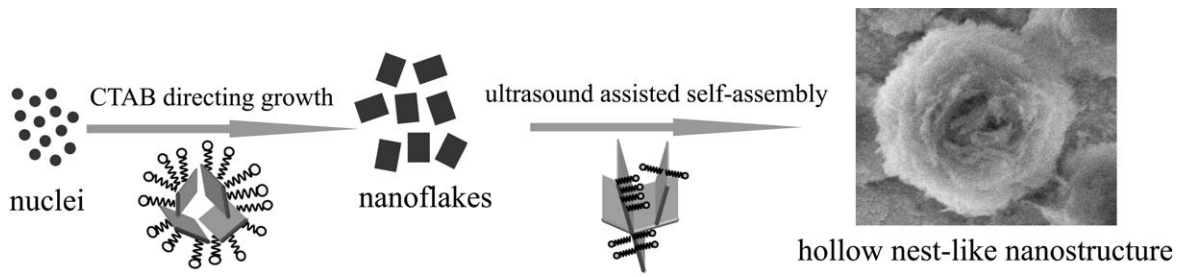

Fig. 4 Schematic illustration of the formation of BaF_2 hollow structure under ultrasonic treatment.

In the presence of EDTA, the strong complexing action between Ba^{2+} ions and EDTA leads to the formation of Ba-EDTA complexes. In the complex, EDTA acts as a hexadentate unit by wrapping itself around the metal ion with four oxygen and two nitrogen atoms and forms several five-membered chelate rings. The formation of the complexes can reduce the concentration of free Ba^{2+} ions in the solution, and slows the reaction rate, which is favorable for the specific growth of BaF_2 crystals.

The amount of the complexing agent also has an influence on the products. Fig. 5c–f show the TEM images of BaF_2 nanocrystals prepared in the presence of different amounts of EDTA with other reaction conditions remaining the same. When the Ba/EDTA molar ratio was chosen as 4 : 1, the product was composed of solid polyhedrons with size of about 1 μm (Fig. 5c). When the Ba/EDTA molar ratio was chosen as 2 : 1, the product appeared as spherical shape with size of about 1 μm (Fig. 5d). Some of spheres showed hollow character and some were solid. If we choose the Ba/EDTA molar ratio of 1 : 1, a hollow nest-like structure with diameter of 900 nm was obtained (Fig. 5e). Further increase of Ba/EDTA molar ratio to 1 : 1.5 could produce a similar hollow structure with size of about 800 nm, but it took 2.5 h to get a precipitate. Through the experimental results, we found that with the decrease of the amount of EDTA, the as-prepared BaF_2 nanocrystals became less uniform and the hollow extent decreased. In the cases containing lower amounts of EDTA, the complexing actions of Ba-EDTA were not complete and the concentrations of free Ba^{2+} ions were higher. So the reaction rates were much higher and the newborn particles grew fast, which may restrain the structure-directing function of EDTA and lead to less uniform and less hollow products.

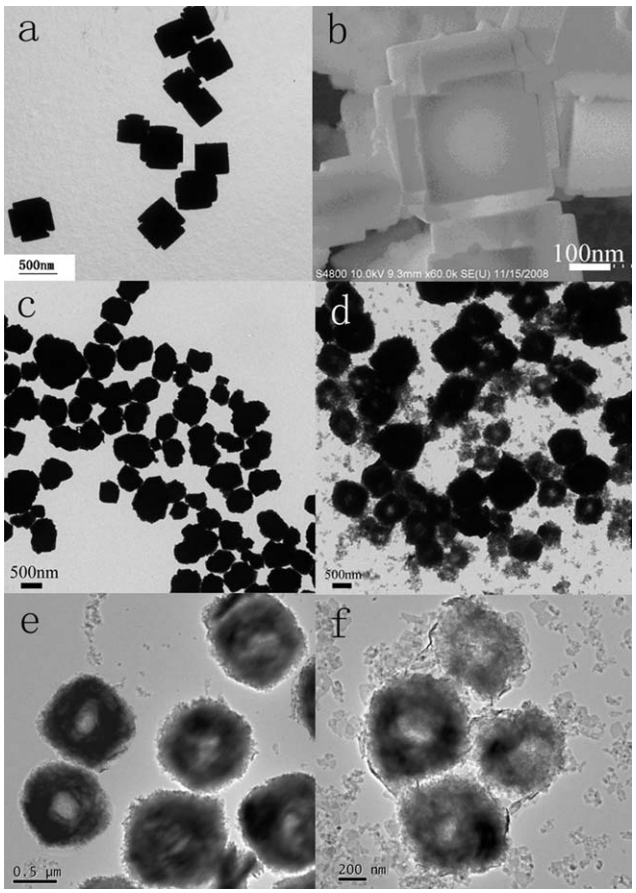

Fig. 5 (a) TEM and (b) SEM image of BaF_2 nanocubes obtained in the reaction system without EDTA, and TEM images of BaF_2 product with a Ba/EDTA molar ratio of (c) 4 : 1, (d) 2 : 1, (e) 1 : 1, and (f) 1 : 1.5.

However, if more EDTA was added, for example, the Ba/EDTA molar ratio was chosen as 1 : 2, there was little precipitate even after the reaction solution was exposed to high-intensity ultrasound irradiation for 2.5 h. The slow reaction speed and the small amount of product might come from the strong coordination between Ba^{2+} and the large amount of EDTA, which may lead to difficulty in release of Ba^{2+} from the complex and the extremely low concentration of available Ba^{2+} to form BaF_2 nuclei. The relationship between the EDTA concentration and the products has been summarized in Table 1. From the above experiments, one can find that the appropriate amount of EDTA plays an important role in the formation of BaF_2 hollow nanocrystals.

3.4 Effect of CTAB concentration

As the structure-directing agent, CTAB was another key factor in the synthesis of the hollow BaF_2 nanostructure. As is known, CTAB is a cationic surfactant, and variation in CTAB concentration will lead to different micelle shapes and invariably affect the morphology of the final product.[19]

Fig. 6 shows the TEM images of BaF_2 nanocrystals prepared in the presence of different amounts of CTAB with the Ba/EDTA molar ratio remaining 1 : 1. In the system without CTAB, 10 nm BaF_2 nanoparticles and their spherical aggregation were obtained, as shown in Fig. 6a. In this case, the absence of surfactant and the high surface energy of small particles resulted in an aggregated product. A lower CTAB amount (0.025 g) gave small nanoflakes (Fig. 6b). This concentration is below the critical micelle concentration of CTAB (CMC, 0.033 g per 100 mL, 30 °C),[20] in which case CTAB exists as single chains and might only work as a capping reagent. The preferential adsorption mechanism is predominant leading to the formation of solid particles. A higher CTAB quantity of 0.1 g resulted in a mixture of hollow and solid spheres (Fig. 6c). When the amount of CTAB was increased to 0.5 g, products appeared as hollow nest-like structure (Fig. 2). In these two situations, CTAB concentrations are higher than the CMC, we presume that the micelles formed and adorption together with the template mechanism might work. It was expected that when the CTAB amount was increased from 0.1 to 0.5 g, the probability for the formation of large CTAB micelle aggregates would increase, leading to the transition of the BaF_2 products from solid to hollow structures. However, when the CTAB concentration was increased to 1 g, in addition to the formation of larger hollow structures, some small BaF_2 solid particles would also appear (Fig. 6d) as the result of excessive adsorption of CTAB on the surfaces of BaF_2 nuclei preventing their further growth. In short, the CTAB adsorption and micellar template mechanism determined the formation of different BaF_2 nanostructures.

Here, ultrasound irradiation might also have an effect on the micellar formation. The ultrasonic irradiation method is an effective method to induce emulsification and the formation of vesicles in the liquid–liquid heterogeneous system and has been

Table 1 The products obtained with different EDTA concentrations

Ba/EDTA molar ratio	1 : 2	1 : 1.5	1 : 1	2 : 1	4 : 1
Obtained product	Little amount of precipitate	Hollow nest-like structure with size of about 800 nm	Hollow nest-like structure with size of about 900 nm	Hollow and solid product with irregular size	Solid product with irregular size
Sonication time	Above 2.5 h	2.5 h	1.5 h	1.5 h	1.5 h
Conclusion			Optimized condition		

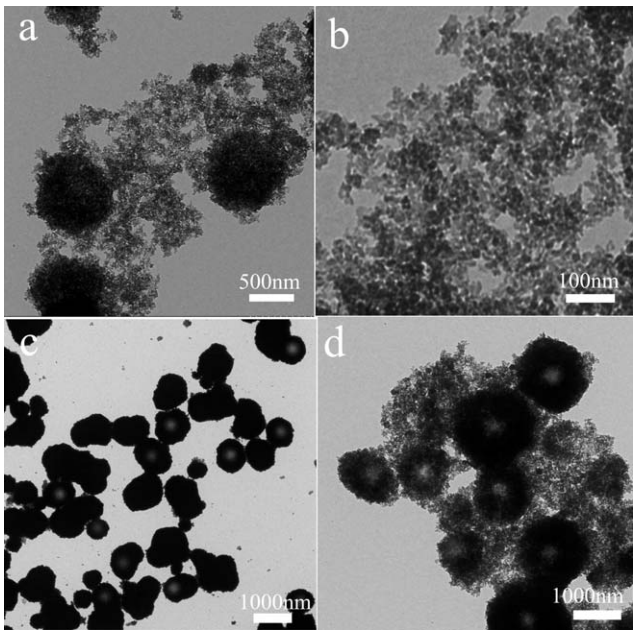

Fig. 6 TEM images of BaF_2 products obtained in reaction systems (a) without CTAB, (b) with 0.025 g CTAB, (c) with 0.1 g CTAB, and (d) with 1 g CTAB.

widely studied.[21] The ultrasound wave might urge the initial self-aggregation of surfactant molecules to form different sized micellar aggregates directly determining the texture of the structures, as has been similarly reported in some literature reports.[22] Also, cavitation and shock waves created by ultrasound can accelerate the primary small flakes to high velocities leading to interparticle collisions and inducing effective self-assembly at the point of collision.[18]

3.5 PL study

Fig. 7a and b are the PL spectra of hollow nest-like structure and solid cubic structure (as shown in Fig. 5a and b, prepared without EDTA) under photon excitation of 300 nm, respectively. As shown in Fig. 7a, the emission peaked at 453 nm, which resulted from an oxygen–vacancy complex with an oxygen on a fluorine site with a next-nearest fluorine vacancy on the surface of the nanocrystals.[23] A weak band at 558 nm could also be detected, which was probably associated with oxygen-vacancy complexes with a nearest fluorine vacancy.[23]

It is interesting that the PL intensity of the hollow structure is much higher than that of the solid cubic structure. These results

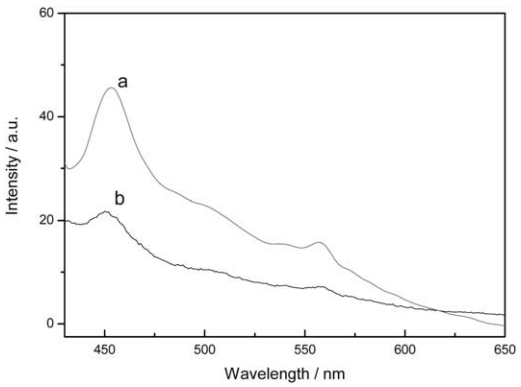

Fig. 7 PL spectrum of (a) the as-prepared BaF_2 hollow nanostructure, (b) the solid cubic product.

indicate that luminescence properties of BaF_2 are very sensitive for its structure and strongly dependent on structural defects. These hollow crystals are expected to exhibit high light-collection efficiency and enhanced luminescence performance due to their hollow structures and large internal surface area at their interior.[12] The enhanced luminescence performance observed in the hollow nanostructure is exciting and may have significant technological applications in the inorganic optical field.

4. Conclusion

In summary, a BaF_2 hollow nest-like nanostructure has been successfully synthesized, for the first time, by using EDTA and CTAB as structure-directing agents *via* a facile sonochemical route. The experimental results showed that complexing reagent EDTA and surfactant CTAB played key roles in the formation of hollow structures. The formation process has been investigated and the ultrasound assisted self-assembly formation mechanism has been proposed. Different morphologies including nanoparticles and nanocubes could also be obtained under controlled reaction conditions. The enhanced green emission observed in the hollow nanostructure is exciting. This unique hollow BaF_2 nest-like structure may be a promising candidate for both fundamental research and functional applications.

Acknowledgements

This work is supported by National Natural Science Foundation of China (Grant No. 20805022, 20821063), China Postdoctoral

Science Foundation (Grant No. 20100471294), and National Basic Research Program of China (Grant 2011CB933502).

Notes and references

1 H. Zeng, J. Li, J. Liu, Z. Wang and S. Sun, *Nature*, 2002, **420**, 395.
2 (*a*) P. Gao and Z. Wang, *J. Am. Chem. Soc.*, 2003, **125**, 11299; (*b*) J. Hu, L. Ren, Y. Guo, H. Liang, A. Cao, L. Wan and C. Bai, *Angew. Chem., Int. Ed.*, 2005, **117**, 1295; (*c*) A. M. Cao, J. S. Hu, H. P. Liang and L. J. Wan, *Angew. Chem., Int. Ed.*, 2005, **44**, 4391.
3 J. Du and Y. Chen, *Angew. Chem., Int. Ed.*, 2004, **43**, 5194.
4 J. H. Bang and K. S. Suslick, *Adv. Mater.*, 2010, **22**, 1039.
5 (*a*) M. Kobayashi, *Solid State Ionics*, 2004, **174**, 57; (*b*) R. Singh, S. Sinha, P. Chou, N. J. Hsu and F. Radpour, *J. Appl. Phys.*, 1989, **66**, 6179.
6 (*a*) A. J. Wojtowicz, *Nucl. Instrum. Methods Phys. Res., Sect. A*, 2002, **486**, 201; (*b*) L. Zhu, J. Meng and X. Q. Cao, *J. Solid State Chem.*, 2007, **180**, 3101.
7 M. H. Cao, C. W. Hu and E. B. Wang, *J. Am. Chem. Soc.*, 2003, **125**, 11196.
8 H. Z. Lian, Z. R. Ye and C. S. Shi, *Nanotechnology*, 2004, **15**, 1455.
9 P. Gao, Y. Xie and Z. Li, *Eur. J. Inorg. Chem.*, 2006, 3261.
10 T. Xie, S. Li, Q. Peng and Y. D. Li, *Angew. Chem., Int. Ed.*, 2009, **48**, 196.
11 F. Caruso, *Chem.–Eur. J.*, 2000, **6**, 413.
12 (*a*) L. F. Gou and C. J. Murphy, *Nano Lett.*, 2003, **3**, 231; (*b*) M. Grätzel, *Nature*, 2001, **414**, 338; (*c*) W. U. Huynh, J. J. Dittmer and A. P. Alivisatos, *Science*, 2002, **295**, 2425; (*d*) S. Nishimura, N. Abrams, B. A. Lewis, L. I. Halaoui, T. E. Mallouk, K. D. Benkstein, J. V. Lagemaat and A. J. Frank, *J. Am. Chem. Soc.*, 2003, **125**, 6306.
13 (*a*) D. E. Zhang, X. J. Zhang, X. M. Ni and H. G. Zheng, *Cryst. Growth Des.*, 2007, **7**, 2117; (*b*) L. Rajput and K. Biradha, *Cryst. Growth Des.*, 2007, **7**, 2376.
14 (*a*) S. H. Yu and H. Colfen, *J. Mater. Chem.*, 2004, **14**, 2124; (*b*) Q. Zhang, S. J. Liu and S. H. Yu, *J. Mater. Chem.*, 2009, **19**, 191.
15 (*a*) K. S. Suslick, *Ultrasound: Its Chemical, Physical and Biological Effects*, VCH, Weinheim, Germany, 1988; (*b*) K. S. Suslick, D. A. Hammerton and R. E. Cline, *J. Am. Chem. Soc.*, 1986, **108**, 5641.
16 T. Sugimoto, *Adv. Colloid Interface Sci.*, 1987, **28**, 65.
17 C. Li, W. Cai, Y. Li, J. Hu and P. Liu, *J. Phys. Chem. B*, 2006, **110**, 1546.
18 S. J. Doktycz and K. S. Suslick, *Science*, 1990, **247**, 1067.
19 (*a*) N. R. Jana, L. Gearheart and C. J. Murphy, *Chem. Commun.*, 2001, 617; (*b*) J. Perez-Juste, L. M. Liz-Marzan, S. Carnie, D. Y. C. Chan and P. Mulvaney, *Adv. Funct. Mater.*, 2004, **14**, 571; (*c*) J. Li, L. Delmotte and H. Kessler, *Chem. Commun.*, 1996, 1023.
20 M. J. Rosen, *Surfactants and Interfacial Phenomena, Second Edition*, Wiley, New York, 1989.
21 (*a*) H. Ringsdorf, B. Schlarb and J. Venzmer, *Angew. Chem., Int. Ed. Engl.*, 1988, **27**, 113; (*b*) E. F. Marques, *Langmuir*, 2000, **16**, 4798.
22 (*a*) S. F. Wang, F. Gu and M. K. Lü, *Langmuir*, 2006, **22**, 398; (*b*) Y. R. Ma, L. M. Qi, J. M. Ma, H. M. Cheng and W. Shen, *Langmuir*, 2003, **19**, 9079; (*c*) X. W. Zheng, Y. Xie, L. Y. Zhu, X. C. Jiang and A. H. Yan, *Ultrason. Sonochem.*, 2002, **9**, 311.
23 U. Rogulis, S. Schweizer and J. M. Spaeth, *J. Phys.: Condens. Matter*, 2002, **14**, 6949.